

TOWARD MINIMAL MISALIGNMENT AT MINIMAL COST IN ONE-STAGE AND ANCHOR-FREE OBJECT DETECTION

Shuaizheng Hao, Hongzhe Liu, Cheng Xu, Songyin Dai

ABSTRACT

Non keypoint-based object detection models consist of classification and regression branches, due to different task drivers, these two branches have different sensibility to the features from the same scale level and the same spatial location. The point-based prediction method, which is based on the assumption that the high classification confidence point has the high regression quality, leads to the misalignment problem. Our analysis shows, the problem is further composed of scale misalignment and spatial misalignment specifically. We aim to resolve the phenomenon at minimal cost—a minor adjustment of the head network and a new label assignment method replacing the rigid one. Our experiments show that, compared to the baseline FCOS, a one-stage and anchor-free object detection model, our model consistently get around 3 AP improvement with different backbones, demonstrating both simplicity and efficiency of our method. Our code will be available at.

Index Terms— Object detection, feature misalignment, label assignment

1. INTRODUCTION

Object detection is a rather developed research filed in the era of deep learning. Two different tasks, classification aiming at researching the differing features across multi classes and regression aiming at drawing the accurate bounding boxes, are often considered. However, due to a huge feature information sensitivity between these two tasks, TSD [1] shows spatial feature misalignment problem exists and compromises the NMS-based models' ability to predict high-confidence classification and high-quality regression results simultaneously.

Typically, multi-stage detection models [2, 3, 4] refine a better aligned result by filling the misalignment gap with fully-connected structures in subsequent stages. Although given a large number of iterations, multi-stage models alleviate the misalignment problem gradually, the cost of a heavy network is far from practical. There is also a difference between anchor-based and anchor-free models in the case of misalignment problem. Compared to anchor-free models, anchor-based models have the choice to assign a single point with one or multiple anchors following Iou assignment rules. During the assignment procedure, anchor-based models have

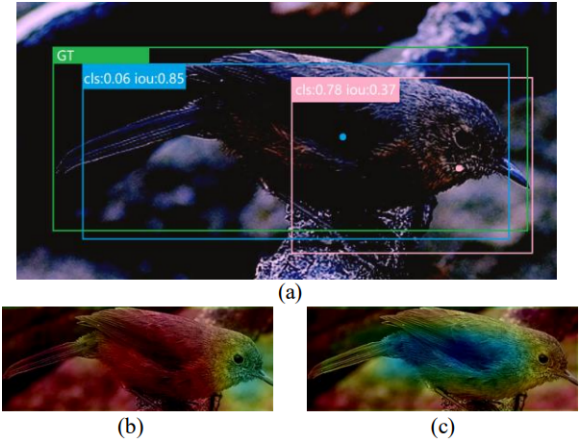


Fig. 1. Illustration of spatial misalignment problem. (a) is the detection results at different spatial locations, (b) and (c) are classification and regression loss distribution respectively. Locations with red color have larger loss than locations with blue color.

the ability to assign positive labels to the most aligned samples naturally. Thus, we pose a question: is there a simple enough method to solve the misalignment problem, especially in one-stage and anchor-free models?

For this reason, we begin to investigate the fundamental structure of the misalignment problem based on FCOS [5]. Beyond spatial feature misalignment, we find there is another one, which we call scale feature misalignment, also leading to the phenomenon. To demonstrate the disparity of scale sensibility in classification and regression branch, we adopt average of classification loss, regression loss and sum of them from each scale level respectively as the scale assignment criteria. The results are in Table 1. When assigned by average classification loss or regression loss alone, models underperform a lot than the model assigned by average sum of them. The disparity of them means there is a myriad of instances whose most acute classification and regression features are not shared by the same scale level. In other words, there is a performance gap between two tasks on the features from the same scale level.

For the spatial misalignment part, we render spatial distributions of classification loss and regression loss within the same instance. As shown in Fig.1, the two distributions are highly misaligned. The points with minuscule classification loss or regression loss have better features for these

Table 1. Models’ performance under different scale assignment standards. “Comb-loss” denotes the combined loss of classification loss and regression loss.

Standard	AP	AP ₅₀	AP ₇₅
Cls_loss	36.7	56.9	39.1
Reg_loss	37.2	55.8	40.1
Comb_loss	38.6	57.5	41.6

two branches to exploit respectively. Thus, the highly misaligned distributions of the loss of two tasks show these two tasks don’t prefer the features at the same spatial locations.

Under these analyses, to solve the scale feature misalignment problem, we design a task-driven dynamic receptive field adaptor, a simple but effective deformable convolution module, for each task. To alleviate the negative effect brought by spatial feature misalignment, we design a label assignment method mining the most spatially aligned samples to strengthen the model’s ability to predicate the reliable regression points with high classification scores.

We summarize our contributions as follows:

1. We revisit and decompose the feature misalignment problem in object detection with two components, confirming the existence of scale misalignment problem, in addition to spatial misalignment one.
2. Based on the observation above, we resolve the problems at minimal cost. With an additive plug-in dynamic receptive filed adaptor (RFA) module as an adjustment of model’s head, and a new label assignment method, aligned feature points sampler (ASP), the two problems are alleviated extensively. Our model, MMMC, is in minimal misalignment at minimal cost, and gets state-of-art performance at (AP), with backbone ()).

2. RELATED WORK

2.1. Scale Misalignment

Since SSD [6] and FPN [7] propose to detect objects with different sizes at different scale levels, there are numerous methods to extract better aligned features for different scale levels. PaNet [8], BiFpn [9] and ASFF [10] merge scale information in a deeper and more complex manner, the performance gap between two tasks is mitigated as each scale level includes more comprehensive information from other scale levels. Recursive-Fpn [11] uses ASPP [12] structure to merge information across scale levels, also mitigating the performance gap between two tasks. Nas-Fpn [13] searches the best merging route horizontally and vertically from a huge searchable space. All these methods refine better aligned features on scale level, but their calculation cost is also huge.

2.2. Spatial Misalignment

Rcnn models [2, 3] use two fully-connected structures to extract different features from the same proposals in the second stage for two tasks, alleviating spatial misalignment problem

at some degree. Cascade Rcnn [4] iterate the process of Rcnn at multiple times, thus refining more spatially aligned features for these two different tasks. TSD [1] resolves the problem with lighter cost, by extracting features from two different proposals for classification and regression respectively. However, all these methods fail to apply in modern one-stage detectors.

Regression qualities prediction is also a common-used method. The multiplication result of classification score and regression score is a better standard in NMS procedure compared to classification alone. Iou-Net [14] is the first network learning to predict regression qualities at different proposals. Iou-Aware [15] and PAA [16] employ extra iou prediction branch to suggest regression-reliable points in one-stage models. Similarly, FCOS [5] has a centerness score prediction branch to represent regression qualities. VFNet [17] merges regression quality prediction branch directly with classification head, by setting Iou scores as soft labels for classification head.

Recently, label assignment is found efficient to improve performance without inferencing cost. ATSS [18] calculates iou threshold for each instance based on the statistics of iou between bounding box and anchor boxes. PAA [16] considers the sum of loss from two branches as cluster standard, mining balanced sampling points and anchors for each instance in training procedure. OTA [19] assigns labels in an overall way for each input image, its assignment results are based on optimal transportation theory. These assignment methods inadvertently help model mine spatially aligned points at some degree, but their strategies confine positive samples to instances’ center regions.

3. PROPOSAL

3.1. dynamic receptive filed adaptor

In the heads of modern one-stage detectors, to get feature map with identical size across two branches, each step of four convolutional operations from two branches shares exactly the same kernel size, striding and padding. The final receptive filed of each branch is calculated by:

$$\begin{cases} \mathcal{R}_{cls} = f(\mathcal{R}_l) \\ \mathcal{R}_{reg} = f(\mathcal{R}_l) \end{cases} \quad (1)$$

\mathcal{R}_l is the receptive field over input image of initial feature map fed by each FPN level, $f(\bullet)$ is a static calculation method about receptive filed across four sequential convolution layers. Due to the same configurations in the two branches and the static $f(\bullet)$, the receptive filed of each branch is identical and static. To drive two branches to take different scale information automatically under the same scale level, we replace the first convolution procedure with deformable convolution, considering the latter has the ability to dynamically adjust re-

ceptive filed:

$$\begin{cases} \mathcal{R}_{cls} = f(\mathcal{R}_l, X_l, \theta_{cls}) \\ \mathcal{R}_{reg} = f(\mathcal{R}_l, X_l, \theta_{reg}) \end{cases} \quad (2)$$

X_l is the initial feature map information shared by both tasks, while θ_{cls} and θ_{reg} are parameters provided by deformable convolutions from each branch. Although a simple replacement, this adjustment gives the model ability to adopt individual receptive filed for the individual tasks. Under this configuration, each task-driven branch dynamically extracts its own scale information by tweaking its receptive filed according to detailed feature information and task requirement.

There are also other ways to adjust each branch’s receptive filed, such as placing dilated convolution or adding extra convolutions. Our experiment shows these methods also work as the disparity of scale misalignment is diminished. However, if such, the receptive filed of each branch is static no matter how different each instance is, and model loses the ability to adapt to different information spatially. With deformable convolution, each point of feature map has different receptive filed for different instances in theory:

$$\begin{cases} \mathcal{R}_{cls}^i = f(\mathcal{R}_l, X_l^i, \theta_{cls}) \\ \mathcal{R}_{reg}^i = f(\mathcal{R}_l, X_l^i, \theta_{reg}) \end{cases} \quad (3)$$

It is noticeable that our RFA module is only applied in the first step of detector’s head, with two individual deformable convolutions to augment each branch’s adaption ability about scale information, and further mitigating the disparity of scale misalignment. It’s different from directly applying deformable convolution to backbones or necks, without considering different receptive filed for two branches. It also differs from VFNet [17] and RepPoints [20], which merge the information of two branches by deformable convolution. In our case, each branch is liberalized of scale mismatch as we enable each feature point in each branch with different and individual receptive filed according to detailed feature information.

3.2. aligned feature points sampler

Traditionally, anchor-based methods assign positive labels to instances simultaneously on scale level and spatial location according to pre-defined iou threshold, while anchor-free models [21, 22] decompose assignment scheme to scale assignment and spatial assignment procedure, both of which rely on extra hyperparameters. These extra hyperparameters mean the models could not adapt to different instances automatically, and they fail to take misalignment problem into consideration. In order to resolve the feature misalignment problem according to instances’ features dynamically, we design a comprehensive and hyperparameter-single label assignment scheme to mine the most aligned scale levels and spatial locations for each instance sequentially.

Aligned Scales Assignment Procedure. For one input image, we define F_l as the feature map fed by each FPN level.

For each instance \mathcal{I}_i from the input, we define P_l as the feature points within bounding box of \mathcal{I}_i from corresponding fpn level. The number of candidate points for each scale level is limited within \mathcal{K} :

$$N_l = \max(\mathcal{K}, \sum_i |P_l^i \in F_l|) \quad (4)$$

Given candidate numbers N_l for each level, we choose candidate points C_l based on their summed loss of two branches without spatial confinement:

$$C_l = \left\{ \arg \min_{P_i \in P_l} N_l (\mathcal{L}_{cls}^i + \mathcal{L}_{reg}^i) \right\} \quad (5)$$

Following typical assignment strategies, we assign each instance to two scale levels to meet the demand of model’s generality on scale dimension. In our case, instead of assigning by Iou thresholds or scale range hyperparameters, we assign directly by the average loss of each scale level forwarded by the same instance \mathcal{I}_i . The assignment results are calculated by:

$$l^* = \arg \min_l 2 \sum_i^{N_l} (\mathcal{L}_{cls}^i + \mathcal{L}_{reg}^i) / N_l \quad (6)$$

That is given by the intuition: given one instance, the average loss reflects the preference degree for model itself about each scale level. Under this assignment standard, the assigned scale levels are no longer purely driven by instances’ sizes and determined by models’ preference automatically. Further, we take into scale misalignment problem into consideration, the assignment standard is a balanced sum of classification loss and regression loss.

Aligned Spatial Points Assignment Procedure. Given scale assignment result l^* for each instance \mathcal{I}_i , and candidate points C_{l^*} from l^* , the task for us is to further mine the most spatially aligned points from C_{l^*} . There are two metrics to be considered for each candidate point: (1) the overall fitness degree S_f under consideration of both tasks; (2) the misaligned degree S_m caused by misaligned loss distributions on space as we mentioned in section1. We evaluate S_f as formulated in the equation, which consist of adoption score of both tasks:

$$S_f(\mathcal{L}_{cls}, \mathcal{L}_{reg}) = \frac{\exp(\mathcal{L}_{cls})}{\sum_j \exp(\mathcal{L}_{cls}^j)} + \frac{\exp(\mathcal{L}_{reg})}{\sum_j \exp(\mathcal{L}_{reg}^j)} \quad (7)$$

Fig.2. We use softmax function to redistribute \mathcal{L}_{cls} and \mathcal{L}_{reg} into the same measurable standard separately, that is given by the advantage that softmax function is monotone and the sum of its output is one. For misaligned degree S_m , as we find sigmoid function is highly efficient converting variant input into a rather unified output, we define it as followings:

$$S_m(\mathcal{L}_{cls}, \mathcal{L}_{reg}) = \begin{cases} \frac{1}{1+\exp(\mathcal{L}_{cls}-\mathcal{L}_{reg})}, \mathcal{L}_{cls} > \mathcal{L}_{reg} \\ \frac{1}{1+\exp(\mathcal{L}_{reg}-\mathcal{L}_{cls})}, \mathcal{L}_{reg} > \mathcal{L}_{cls} \end{cases} \quad (8)$$

If only assigning labels according to the S_f , model may be involved in over-fitting problem as only the easiest samples are assigned with positive labels. On the other side, if

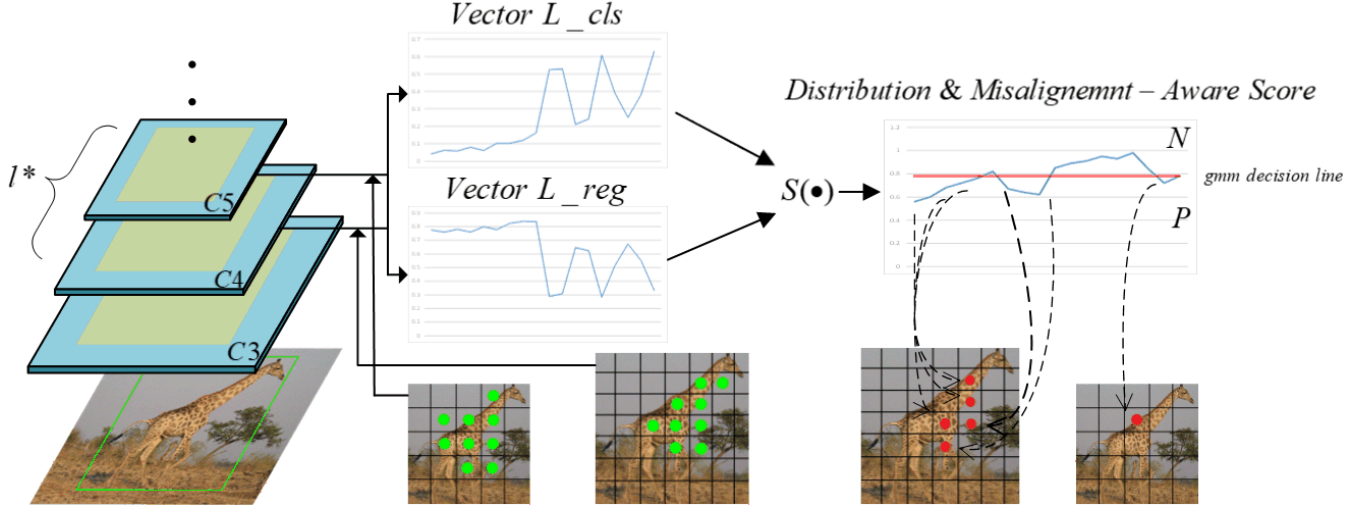


Fig. 2. An illustration of aligned feature points sampling procedure. Vectors L-cls , L-reg are pair-wise and chosen from the same spatial locations orderly. We compute distribution and misalignment-aware outcome from these two vectors, the final assignment results are given by Gaussian Mixture Model (GMM).

only assigning labels according to S_m , model would fail to converge during training as it could not find a consistent convex point. Given the analyses above, we define the final score of candidate points C_{l^*} as the square root of the multiply of fitness degree S_f and misalignment degree S_m :

$$S = \sqrt{S_f * S_m} \quad (9)$$

The final score S is both balanced and misalignment-aware of two tasks. The decision of positive points P and negative points N from candidate points C_{l^*} according to S is based on gmm, as its ability to dynamically draw decision line according to scores distribution. The final spatial assign result is formulated as:

$$P, N = gmm(S) \quad (10)$$

In our case, we find the distribution of evaluated final score S of different instances vary a lot, especially in early iterations. Compared to simply assign in topK manner, gmm have a better performance as with convergence.

4. EXPERIMENTS

In this section we conduct our experiments on COCO benchmark. Following the common practice, we use trainval35k set (115k images) as train set and evaluate on coco val set (5k images) for ablation studies. Extensive experiments are evaluated on test-dev set (20k images) to compare with the state-of-art models.

4.1. implementation details

We use ResNet-50 pre-trained on ImageNet and FPN as our backbone and neck for our ablation studies, if not specified.

Synchronized stochastic gradient (SGD) is employed on 8 GPUs with mini-batch set to 16. The model is trained with 90k iterations. The initial learning rate is 0.01 and is decayed by a factor of 10 after 60k and 80k iterations. To make sure shorter edge of input images is 800, and longer edge no more than 1333, input images are resized before feeding into the model. Following other common practice, we use Focal Loss [21] and Giou Loss [22] for classification task and regression task respectively. As recent researches [23, 17] shows, centerness has some shortcomings for predicting regression qualities. We simply replace the supervision signal with giou and set BCE Loss for the regression quality predicting branch. As for label assignment scheme, we set \mathcal{K} to 9 and GMM's minimum and maximum score of the candidate points are set by mean of the two components.

4.2. ablation study

Effects of individual components. In this section we verify the effectiveness of each component of our proposal. Receptive Filed Adaptor (RFA) and Aligned Point Sampler (APS) is gradually added to the baseline to make a comprehensive comparison and analyses. As shown in the second row in Table 2, without complex network design or a bunch of extra cost, only RFA brings a significant performance improvement around 2 AP, which suggest that the scale misalignment is alleviated by a huge progress. The third row of Table 2 shows APS scheme also lifts the performance by 1.6 AP in a cost-free way. The combined result of RFA and APS get an absolute improvement of 3.1AP, showing both the simplicity and effectiveness of our proposal MMMC.

Plug-in Position of Receptive Filed Adaptor. Our RFA is a simple and plug-in module suitable for most modern object detection head networks. Normally, modern head network

Table 2. Ablation study of Receptive Filed Adaptor (RFA) and Aligned Points Sampler (APS). “*” denotes centerness as auxiliary branch, while others use Giou prediction.

method	RFA	APS	FPS	AP	AP ₅₀	AP ₇₅
FCOS*			14.7	38.6	57.2	41.9
FCOS			14.7	39.4	57.3	42.7
MMMC	✓		14.6	40.5	58.0	44.3
		✓	14.7	40.2	58.2	43.1
	✓	✓	14.6	41.7	59.3	45.1

Table 3. Analysis of plug-in position for RFA in head network.

Position	Cls	Reg	AP	AP ₅₀	AP ₇₅
1	✓	✓	39.8	58.4	43.2
2	✓	✓	39.8	58.3	42.9
3	✓	✓	39.8	57.8	43.0
4	✓	✓	39.9	58.2	43.3

is composed of four sequential convolutional operations. Our RFA module could be applied in anyone of these four to boost the receptive filed adoption ability for two branches separately. Given by the fact RFA is composed of two individual and parallel deformable convolutional operations, there are sixteen configurations in theory. For simplicity, we only compare the combined performance when RFA’s two components are under the same plug-in positions. Table 3 shows RFA is not sensitive to the choice of plug-in positions, suggesting the generality of our proposal.

Why RFA reduces scale misalignment phenomenon. As we talked about in section1, there is a performance gap between two tasks on the features from the same scale level. We consider loss gap and loss sum between two tasks from the same scale level reflect models’ adaption ability on scale information. Thus, we collect the average loss gap and loss sum per instance during one training epoch at model’s different iterations. As shown in Table 4 and Table 5, models with RFA module consistently get around 2% relative reduction on the two metrics at different iterations, showing RFA’s ability on conciliating scale misalignment between two tasks without compromising the whole model’s performance.

Scale and Spatial Label Assignment. Our APS is composed of scale assignment and spatial assignment procedures. As Table 6 shows, when these two procedures are separately adopted, the improvement of model’s performance is minor with 0.3 AP and 0.5 AP boost respectively. However, when the two procedures are combined, model reaches 41.7 AP with an absolute 1.2 AP gain. This synergic effect means each procedure helps the other find the best aligned result on corresponding scale levels or spatial locations.

Visualization of APS’ Spatial Assignment Result. We visualize the spatial distribution of classification and regression loss, and further mark the positive assignment results on the input image in Fig.3. There are two instances in input image,

Table 4. Analysis of loss gap between two branches at different iterations. We compare base model with and without RFA.

iterations	15k	30k	45k	60k	75k
Base_gap	0.169	0.156	0.141	0.150	0.137
Rfa_gap	0.167	0.153	0.149	0.146	0.134
reduction	1.2%	1.9%	1.3%	2.7%	2.2%

Table 5. Analysis of loss sum between two branches at different iterations. We compare base model with and without RFA.

iterations	15k	30k	45k	60k	75k
Base_sum	0.580	0.523	0.487	0.454	0.412
Rfa_sum	0.570	0.511	0.466	0.442	0.401
reduction	1.2%	2.3%	4.5%	2.5%	2.7%

one is spatially aligned and the other is misaligned. Compared to atss and paa, there isn’t significant assignment difference in the spatially aligned instance. While in the spatially misaligned instance, MMC assigns more aligned points with positive label according to loss distribution of each task, than atss and paa does.

Comparison with State-of-the-art Methods. We compare MMC with state-of-the-art detectors on MS COCO test-dev set. We adopt 180k training iterations following the previous works. Results are shown in Table 7. Our model, with tiny extra parameters cost, achieves 45.7% accuracy on Res101 backbone, surpassing previous best anchor-based and anchor-free models.

5. CONCLUSIONS

In this paper we revisit and investigate the fundamental structure of feature misalignment problem in object detection. We analysis the problem is composed of scale and spatial one. For scale misalignment, we propose a plug-in and light module RFA to dynamically tweak each branch’s receptive filed. For spatial misalignment, we propose a novel label assignment scheme mining the most spatially aligned points. Experiments show that our proposal significantly boost model’s performance and the corresponding misalignment problems are alleviated.

6. REFERENCES

- [1] Guanglu Song, Yu Liu, and Xiaogang Wang, “Revisiting the sibling head in object detector,” in *Proceedings of the IEEE/CVF Conference on Computer Vision and Pattern Recognition*, 2020, pp. 11563–11572.
- [2] Shaoqing Ren, Kaiming He, Ross Girshick, and Jian Sun, “Faster r-cnn: Towards real-time object detection with region proposal networks,” *Advances in neural information processing systems*, vol. 28, pp. 91–99, 2015.

Table 6. Ablation study of scale assignment and spatial assignment procedures.

Scale	Spatial	AP	AP ₅₀	AP ₇₅
		40.5	58.0	44.3
✓		40.8	58.9	44.2
	✓	41.0	58.8	45.0
✓	✓	41.7	59.3	45.1

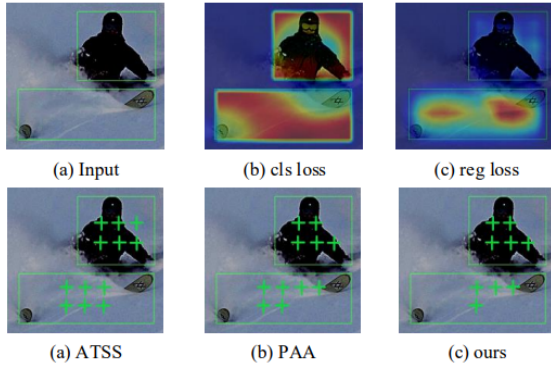


Fig. 3. The visualization of spatial label assignment. The first row shows input and loss distribution of two tasks separately. The green crosses in the second row are positive assignment points.

- [3] Ross Girshick, “Fast r-cnn,” in *Proceedings of the IEEE international conference on computer vision*, 2015, pp. 1440–1448.
- [4] Zhaowei Cai and Nuno Vasconcelos, “Cascade r-cnn: Delving into high quality object detection,” in *Proceedings of the IEEE conference on computer vision and pattern recognition*, 2018, pp. 6154–6162.
- [5] Zhi Tian, Chunhua Shen, Hao Chen, and Tong He, “Fcos: Fully convolutional one-stage object detection,” in *Proceedings of the IEEE/CVF international conference on computer vision*, 2019, pp. 9627–9636.
- [6] Wei Liu, Dragomir Anguelov, Dumitru Erhan, Christian Szegedy, Scott Reed, Cheng-Yang Fu, and Alexander C Berg, “Ssd: Single shot multibox detector,” in *European conference on computer vision*. Springer, 2016, pp. 21–37.
- [7] Tsung-Yi Lin, Piotr Dollár, Ross Girshick, Kaiming He, Bharath Hariharan, and Serge Belongie, “Feature pyramid networks for object detection,” in *Proceedings of the IEEE conference on computer vision and pattern recognition*, 2017, pp. 2117–2125.
- [8] Shu Liu, Lu Qi, Haifang Qin, Jianping Shi, and Jiaya Jia, “Path aggregation network for instance segmentation,” in *Proceedings of the IEEE conference on computer vision and pattern recognition*, 2018, pp. 8759–8768.
- [9] Mingxing Tan, Ruoming Pang, and Quoc V Le, “Efficientdet: Scalable and efficient object detection,” in

Table 7. MMMC vs. the state-of-the-art methods on COCO test-dev set with Res101 backbone.

Method	AP	AP ₅₀	AP ₇₅	AP _S	AP _M	AP _L
FCOS [5]	41.5	60.7	45.0	24.4	44.8	51.6
F.Anchor [24]	41.8	61.1	44.9	23.4	44.9	52.9
SAPD [25]	43.1	62.2	46.4	24.5	46.1	54.8
MAL [26]	43.6	61.8	47.1	25.0	46.9	55.8
ATSS [18]	43.6	62.1	47.4	26.1	47.0	53.6
GFL [27]	45.0	63.7	48.9	27.2	48.8	54.5
PAA [16]	44.8	63.3	48.7	26.5	48.8	56.3
IQ-DET [28]	45.1	63.4	49.3	26.7	48.5	56.5
OTA [19]	45.3	63.5	49.3	26.9	48.8	56.1
MMMC(ours)	45.7	64.0	49.8	27.6	49.2	56.8

Proceedings of the IEEE/CVF conference on computer vision and pattern recognition, 2020, pp. 10781–10790.

- [10] Songtao Liu, Di Huang, and Yunhong Wang, “Learning spatial fusion for single-shot object detection,” *arXiv preprint arXiv:1911.09516*, 2019.
- [11] Siyuan Qiao, Liang-Chieh Chen, and Alan Yuille, “Detectors: Detecting objects with recursive feature pyramid and switchable atrous convolution,” in *Proceedings of the IEEE/CVF Conference on Computer Vision and Pattern Recognition*, 2021, pp. 10213–10224.
- [12] Liang-Chieh Chen, George Papandreou, Iasonas Kokkinos, Kevin Murphy, and Alan L Yuille, “Deeplab: Semantic image segmentation with deep convolutional nets, atrous convolution, and fully connected crfs,” *IEEE transactions on pattern analysis and machine intelligence*, vol. 40, no. 4, pp. 834–848, 2017.
- [13] Golnaz Ghiasi, Tsung-Yi Lin, and Quoc V Le, “Nas-fpn: Learning scalable feature pyramid architecture for object detection,” in *Proceedings of the IEEE/CVF Conference on Computer Vision and Pattern Recognition*, 2019, pp. 7036–7045.
- [14] Borui Jiang, Ruixuan Luo, Jiayuan Mao, Tete Xiao, and Yuning Jiang, “Acquisition of localization confidence for accurate object detection,” in *Proceedings of the European conference on computer vision (ECCV)*, 2018, pp. 784–799.
- [15] Shengkai Wu, Xiaoping Li, and Xinggang Wang, “Iou-aware single-stage object detector for accurate localization,” *Image and Vision Computing*, vol. 97, pp. 103911, 2020.
- [16] Kang Kim and Hee Seok Lee, “Probabilistic anchor assignment with iou prediction for object detection,” in *Computer Vision—ECCV 2020: 16th European Conference, Glasgow, UK, August 23–28, 2020, Proceedings, Part XXV 16*. Springer, 2020, pp. 355–371.
- [17] Haoyang Zhang, Ying Wang, Feras Dayoub, and Niko Sunderhauf, “Varifocalnet: An iou-aware dense object detector,” in *Proceedings of the IEEE/CVF Conference*

- on Computer Vision and Pattern Recognition*, 2021, pp. 8514–8523.
- [18] Shifeng Zhang, Cheng Chi, Yongqiang Yao, Zhen Lei, and Stan Z Li, “Bridging the gap between anchor-based and anchor-free detection via adaptive training sample selection,” in *Proceedings of the IEEE/CVF conference on computer vision and pattern recognition*, 2020, pp. 9759–9768.
- [19] Zheng Ge, Songtao Liu, Zeming Li, Osamu Yoshie, and Jian Sun, “Ota: Optimal transport assignment for object detection,” in *Proceedings of the IEEE/CVF Conference on Computer Vision and Pattern Recognition*, 2021, pp. 303–312.
- [20] Ze Yang, Shaohui Liu, Han Hu, Liwei Wang, and Stephen Lin, “Reppoints: Point set representation for object detection,” in *Proceedings of the IEEE/CVF International Conference on Computer Vision*, 2019, pp. 9657–9666.
- [21] Tsung-Yi Lin, Priya Goyal, Ross Girshick, Kaiming He, and Piotr Dollár, “Focal loss for dense object detection,” in *Proceedings of the IEEE international conference on computer vision*, 2017, pp. 2980–2988.
- [22] Hamid Rezaatofighi, Nathan Tsoi, JunYoung Gwak, Amir Sadeghian, Ian Reid, and Silvio Savarese, “Generalized intersection over union: A metric and a loss for bounding box regression,” in *Proceedings of the IEEE/CVF Conference on Computer Vision and Pattern Recognition*, 2019, pp. 658–666.
- [23] Xiang Li, Wenhai Wang, Lijun Wu, Shuo Chen, Xiaolin Hu, Jun Li, Jinhui Tang, and Jian Yang, “Generalized focal loss: Learning qualified and distributed bounding boxes for dense object detection,” *arXiv preprint arXiv:2006.04388*, 2020.
- [24] Xiaosong Zhang, Fang Wan, Chang Liu, Xiangyang Ji, and Qixiang Ye, “Learning to match anchors for visual object detection,” *IEEE Transactions on Pattern Analysis and Machine Intelligence*, 2021.
- [25] Chenchen Zhu, Fangyi Chen, Zhiqiang Shen, and Marios Savvides, “Soft anchor-point object detection,” in *Computer Vision—ECCV 2020: 16th European Conference, Glasgow, UK, August 23–28, 2020, Proceedings, Part IX 16*. Springer, 2020, pp. 91–107.
- [26] Wei Ke, Tianliang Zhang, Zeyi Huang, Qixiang Ye, Jianzhuang Liu, and Dong Huang, “Multiple anchor learning for visual object detection,” in *Proceedings of the IEEE/CVF Conference on Computer Vision and Pattern Recognition*, 2020, pp. 10206–10215.
- [27] Xiang Li, Wenhai Wang, Lijun Wu, Shuo Chen, Xiaolin Hu, Jun Li, Jinhui Tang, and Jian Yang, “Generalized focal loss: Learning qualified and distributed bounding boxes for dense object detection,” *arXiv preprint arXiv:2006.04388*, 2020.
- [28] Yuchen Ma, Songtao Liu, Zeming Li, and Jian Sun, “Iqdet: Instance-wise quality distribution sampling for object detection,” in *Proceedings of the IEEE/CVF Conference on Computer Vision and Pattern Recognition*, 2021, pp. 1717–1725.